

1 **Superior CO₂/N₂ Separation Performance of High Branched Poly(1,3 dioxolane) Plasticized**
2 **by Polyethylene Glycol**

3

4 Wenji Guo, Thien N. Tran, Himangshu Mondal, Skye Schaefer, Liang Huang*,
5 and Haiqing Lin*

6

7 Department of Chemical and Biological Engineering, University at Buffalo, The State University
8 of New York, Buffalo, NY 14260, USA

9

10 * Corresponding authors:

11 H. Lin, Email: haiqingl@buffalo.edu

12 L. Huang, Email: huangliang0228@163.com

13

14

15

16

17

Revised submission to *Journal of Membrane Science*

18

19 **Abstract**

20 With its high content of CO₂-philic ether oxygen groups, poly(1,3-dioxolane) (PDXLA)
21 has emerged as an attractive platform to achieve excellent CO₂/N₂ separation properties for post-
22 combustion carbon capture. Herein we demonstrate that the separation properties of PDXLA can
23 be further enhanced by plasticizing with miscible polyethylene glycol (PEG)-based additives using
24 an integrated experimentation and modeling approach. The effects of the chain end groups and
25 loading level of the additives on the physical properties of the blends are thoroughly investigated,
26 including glass transition temperature (T_g), fractional free volume, and gas transport properties,
27 and the effects can be satisfactorily described using models available for homogeneous blends.
28 Notably, a T_g -integrated free volume model is adapted to successfully interpret the unified effect
29 of the blend composition and temperature on gas diffusivity and permeability. A sample containing
30 45 mass% PEG dimethyl ether (PEGDME with a molecular mass of 240 g/mol) displays stable
31 mixed-gas CO₂ permeability of 1540 Barrer and CO₂/N₂ selectivity of 40 when challenged with a
32 model flue gas at 60 °C, outperforming Robeson's 2008 upper bound. Elucidating how small
33 plasticizers impact gas transport in homogeneous blends may unravel a facile way to design high-
34 performance membranes for gas separations.

35

36 **Keywords:** poly(1,3-dioxolane); CO₂/N₂ separation membranes; T_g -integrated free volume model;
37 polyethylene glycol dimethyl ether; plasticizer

38

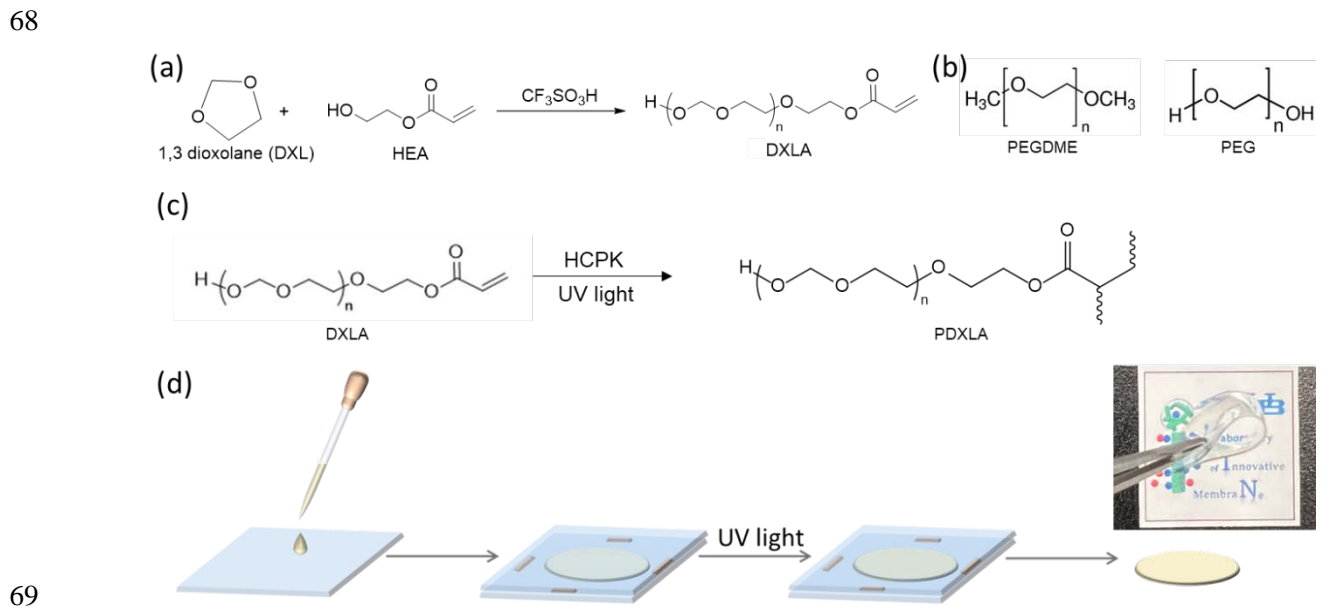
39 1. Introduction

40 Membrane technology has become a leading approach for CO₂ capture from fossil fuel-
41 derived flue gas (or CO₂/N₂ separation) to reduce the CO₂ emissions to the atmosphere because of
42 its inherent advantages, such as great energy efficiency, absence of chemical wastes, low
43 maintenance, and small footprint [1-4]. To realize their practical applications, membrane materials
44 should exhibit high CO₂ permeability and CO₂/N₂ selectivity.

45 Poly(ethylene oxide) (PEO)-based materials have attracted significant interest for CO₂/N₂
46 separation because of their low glass transition temperature (T_g) (yielding flexible chains and thus
47 high gas diffusivity) and strong affinity towards CO₂ (inducing high solubility selectivity and thus
48 high permeability selectivity) [5, 6], such as cross-linked PEO [7-10] and block copolymers [11-
49 13]. These PEO-based materials can be further dispersed with nanoporous nanoparticles (NPs) to
50 form mixed matrix materials with enhanced CO₂/N₂ separation performance, such as metal-
51 organic frameworks (MOFs) or metal-organic polyhedra (MOPs) with high porosity and gas
52 permeability [2, 14-18]. However, it is still challenging to eliminate the interfacial voids between
53 the polymers and NPs, which tend to decrease gas selectivity [16].

54 PEO-based materials have also been augmented with miscible small molecules to improve
55 gas permeability, such as liquid polyethylene glycol (PEG) [14, 19-22], PEG dimethyl ether
56 (PEGDME) [17, 23-28], crown ether [29], salts [30], and carboxylic acids [31]. The addition of
57 the small molecules plasticizes the polymers, decreasing the T_g and increasing the CO₂ diffusivity.
58 For instance, adding 60 mass% 18-Crown-6 in a cross-linked PEO decreased T_g from -61 to -74 °C
59 and increased CO₂ permeability from 600 to 1340 Barrer (1 Barrer = 10⁻¹⁰ cm³(STP) cm cm⁻² s⁻¹
60 cmHg⁻¹) while the CO₂/N₂ selectivity varied from 51 to 48 [29].

61 We have recently reported highly branched poly(1,3 dioxolane) (PDXLA) with higher
 62 contents of ether oxygen groups than PEO and thus superior CO₂/N₂ separation properties to PEO
 63 [32-34]. Figure 1a illustrates the synthesis of the macromonomer (DXLA) from 1,3 dioxolane,
 64 which is then photopolymerized to form PDXLA (Figure 1c,d). The repeating units in the DXLA
 65 can be varied from 5 to 16, and the obtained polymers are amorphous. Increasing the repeating
 66 unit number (*n*) increases gas permeability before leveling off at *n* = 8 [33]. Therefore, DXLA
 67 with *n* = 8 is selected for this study.



69
 70
 71 **Figure 1.** (a) Procedures to synthesize DXLA. (b) Chemical structures of PEGDME and PEG. (c)
 72 Photopolymerization of DXLA to form PDXLA. (d) Schematic of the preparation of PDXLA films
 73 with a photo of a DME240-45 film. More photos of the films are shown in Figure S1.
 74

75 Herein we demonstrate that PDXLA can be plasticized with liquid additives to form
 76 homogeneous blends with improved CO₂/N₂ separation performance. Specifically, three PEGs
 77 with similar chemical structures are investigated, including PEG with molecular mass (M_n) of 400
 78 g/mol (PEG400) and PEGDME with M_n of 240 and 500 g/mol (denoted as PEGDME240 and
 79 PEGDME500, respectively). The physical properties and pure-gas separation properties of these

80 blends were thoroughly characterized. The effect of the additive content on gas diffusivity and
81 permeability can be satisfactorily described using a T_g -integrated free volume model, which has a
82 form similar to Vogel-Tammann-Fulcher (VTF) equation used to describe ion transport.
83 PEGDME240 is the most effective to improve gas permeability among the three additives studied.
84 The sample containing 45 mass% PEGDME240 (DME240-45) renders the best CO₂/N₂ separation
85 properties. When evaluated with model flue gas, it exhibits robust separation properties above
86 Robeson's 2008 upper bound.

87

88 **2. Experimental**

89 **2.1. Materials**

90 1,3-Dioxolane (DXL), 1-hydroxycyclohexyl phenyl ketone (HCPK), PEGDME500, and
91 PEG400 were purchased from Sigma-Aldrich Corporation (St. Louis, MO). 2-Hydroxyethyl
92 acrylate (HEA) and triflic acid (TfOH) were obtained from Acros Organics (Fair Lawn, NJ).
93 PEGDME240 was procured from TCI Chemical Trading Co. (Chuo-ku, Tokyo, JP).
94 Dichloromethane (DCM) was acquired from Fisher Scientific (Hampton, NH) and dried with 3A
95 molecular sieves (Acros Organics) before use. CO₂, He, and N₂ (99.9%) were supplied by Airgas,
96 Inc. (Radnor, PA), and C₂H₆ (99.9%) was purchased from Jackson Welding and Gas Products
97 (Rochester, NY).

98 **2.2. Synthesis of DXLA and PDXLA-based polymers**

99 DXLA was synthesized by cationic ring-opening polymerization of DXL following the
100 procedures described in our previous work (cf. Figure 1a) [32, 33]. TfOH and HEA were used as
101 an initiator and a co-initiator (or chain transfer reagent), respectively. The molar ratio of DXL to
102 HEA was controlled at 8.0 to obtain DXLA with a repeating unit of ≈ 8 . To fabricate PDXLA-

103 based blends, the DXLA was mixed with HCPK (0.1 mass%) and the desired amount of the
104 additive (*i.e.*, PEGDME or PEG). The solution was formed into thin films with a controlled
105 thickness ($\approx 250 \mu\text{m}$) before photopolymerization using 254-nm UV light and procedures
106 described elsewhere [9]. The samples containing PEGDME240, PEGDME500, and PEG400 are
107 denoted as DME240-xx, DME500-xx, or PEG400-xx, respectively, where xx represents the mass
108 percentage of the additive in the blends.

109 **2.3. Characterization of DXLA and the PDXLA-based polymers**

110 A Varian Inova 500 MHz NMR spectrometer was used to characterize the DXLA samples.
111 A Fourier transform infrared (FTIR) spectrometer (Vertex 70 Bruker, Billerica, MA) with
112 attenuated total reflection (ATR) was employed. Differential Scanning Calorimetry (DSC, Q2000,
113 TA Instruments, New Castle, DE) was used to determine thermal transitions. The polymers were
114 heated from $-90 \text{ }^\circ\text{C}$ to $80 \text{ }^\circ\text{C}$ at $10 \text{ }^\circ\text{C min}^{-1}$ before quenching in the N_2 atmosphere for three cycles,
115 and the third heating cycle was used to derive the properties. The density of the films was
116 determined using Mettler Toledo XS64 analytical balance with a density measurement kit [29, 33].
117 Decane was used as the auxiliary liquid because it is non-polar and has very low sorption in the
118 polar PDXLA-based films. The initial mass readings in decane were used for calculation to further
119 avoid the interference by the decane sorption in the films. For each sample, more than three films
120 were measured, and the average density value is reported with the standard deviation.

121 **2.4. Determination of gas transport properties**

122 Constant-volume and variable-pressure apparatus were employed to determine pure-gas
123 permeability (P_A) at temperatures (T) ranging from 23 to $60 \text{ }^\circ\text{C}$ [32]. The leak rate of the system
124 $[(dp_{I,A}/dt)_{\text{leak}}, \text{cmHg/s}]$ was measured at the beginning of the permeation test, and the steady-state

125 pressure increasing rate in the downstream volume $[(dp_{1,A}/dt)_{ss}, \text{cmHg/s}]$ was recorded after the
126 feed pressure ($p_{2,A}$, bar) was applied. The P_A was calculated using Equation 1:

$$127 \quad P_A = \frac{V_d l}{p_{2,A} A R T} \left[\left(\frac{dp_{1,A}}{dt} \right)_{ss} - \left(\frac{dp_{1,A}}{dt} \right)_{leak} \right] \quad (1)$$

128 where V_d is the downstream volume (cm^3), l is the film thickness (cm), A is the film area (cm^2),
129 and R is the gas constant.

130 Constant-pressure and variable-volume apparatus were employed to determine mixed-gas
131 permeability using a gas mixture containing was 20% CO_2 and 80% N_2 [29, 32]. Helium with a
132 flow rate of S was used to sweep the permeated gas to a Micro GC for analysis (Inficon Inc.,
133 Syracuse, NY). Mixed-gas permeability was calculated using Equation 2:

$$134 \quad P_A = \frac{x_A S l}{x_{He} A (p_{2,A} - p_{1,A})} \quad (2)$$

135 where x_A and x_{He} refer to the molar fraction of gas A and helium in the sweep-out stream,
136 respectively.

137 Dual-volume and dual-transducer apparatus were used to determine gas sorption isotherms
138 in the polymers based on a pressure decay method [33]. The sample (3-4 g) was kept in a sample
139 cell. When a known amount of the gas was introduced to the cell, the pressure decreased, and the
140 pressure change can be used to calculate the gas sorption by the samples ($C_A, \text{cm}^3(\text{STP}) \text{atm}^{-1}$).
141 Gas solubility coefficient (S_A) at the equilibrium pressure (p_A , atm) is calculated using Equation 3:

$$142 \quad S_A = C_A / p_A \quad (3)$$

143 Gas diffusivity coefficient ($D_A, \text{cm}^2 \text{s}^{-1}$) in polymers is usually calculated using Equation 4 [3]:

$$144 \quad D_A = P_A / S_A \quad (4)$$

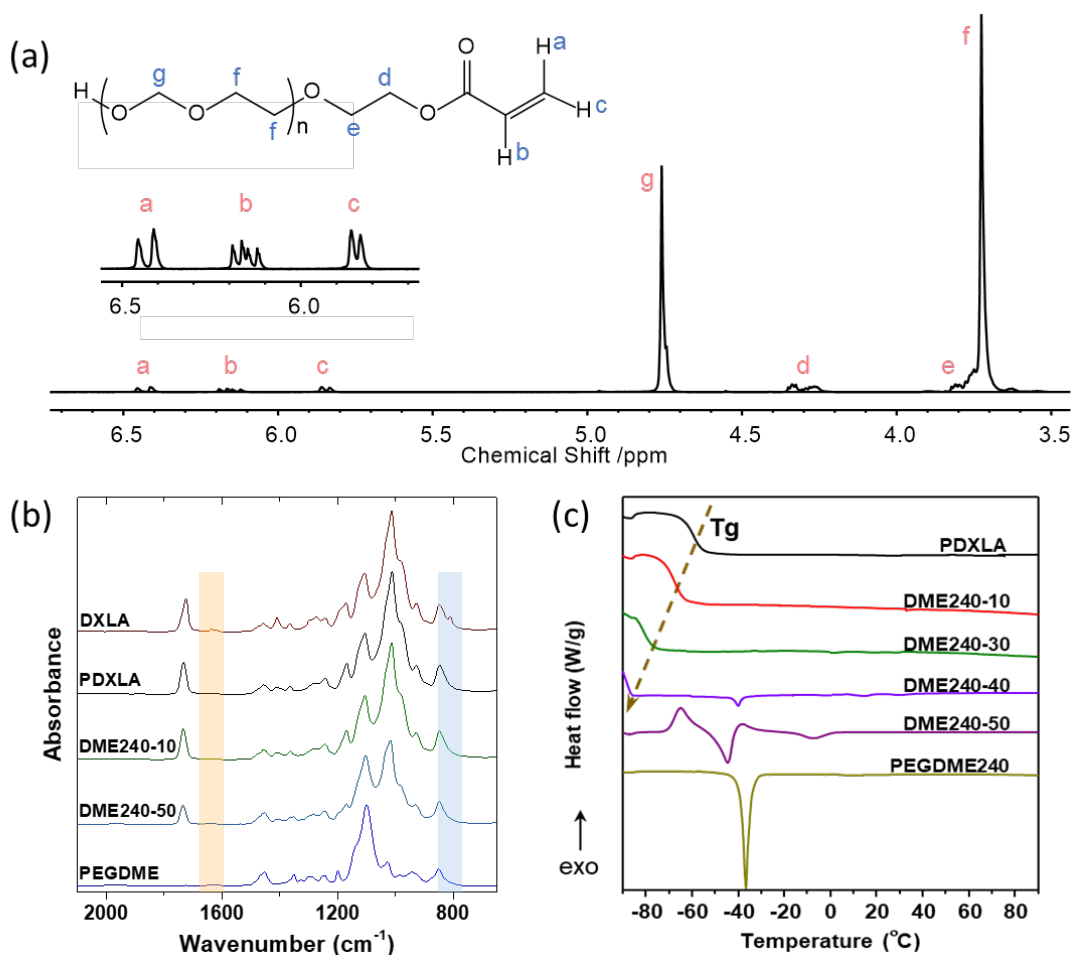
145

146 **3. Results and discussion**

147 **3.1. Physical properties of the PDXLA-based blends**

148 Figure 2a shows the ^1H NMR spectrum of DXLA and the assignment of the chemical shifts
 149 for the protons. The n value of DXLA is the ratio of the resonance intensities of protons from DXL
 150 units (chemical shifts at 3.73 and 4.73 ppm) to those of α -acryloyl protons (chemical shifts at 5.82,
 151 6.13, and 6.42 ppm). The n value for the synthesized DXLA is ≈ 8 , consistent with the ratio of the
 152 monomer (DXL) to the initiator (HEA).

153



154 **Figure 2.** Chemical structure and physical properties of DXLA and the PDXLA-based blends. (a)
 155 ^1H NMR spectrum of DXLA. (b) FTIR spectra of DXLA and DME240-xx. An enlarged image of
 156 the shadowed region is shown in Figure S2. (c) Comparison of DSC curves for the DME240-xx.
 157
 158

159 Figures 2b and S2 compare the FTIR spectra of the representative prepolymer solutions
 160 before and after the photopolymerization, such as DXLA and PDXLA. As shown in Figures 2b

161 and S2, the C=C absorption peaks (810 and 1650 cm^{-1}) in DXLA disappear after the
162 polymerization, suggesting the entire conversion of the DXLA [29, 33]. Additionally, as the
163 PEGDME content increases in the blends, the absorption peaks of the C-O-C stretching (1000 cm^{-1})
164 and C=O stretching (1740 cm^{-1}) in PDXLA decrease. Figure S3 compares the FTIR spectra of the
165 additives, PDXLA, and their blends. PEGDME240 and PEGDME500 exhibit almost the same
166 spectra because of their similar chemical structures. PDXLA displays a peak at 3508 cm^{-1} for the
167 O-H stretching, which red-shifts to 3485 cm^{-1} in PEG400-40, indicating the formation of the
168 hydrogen bonding between PEG400 and PDXLA.

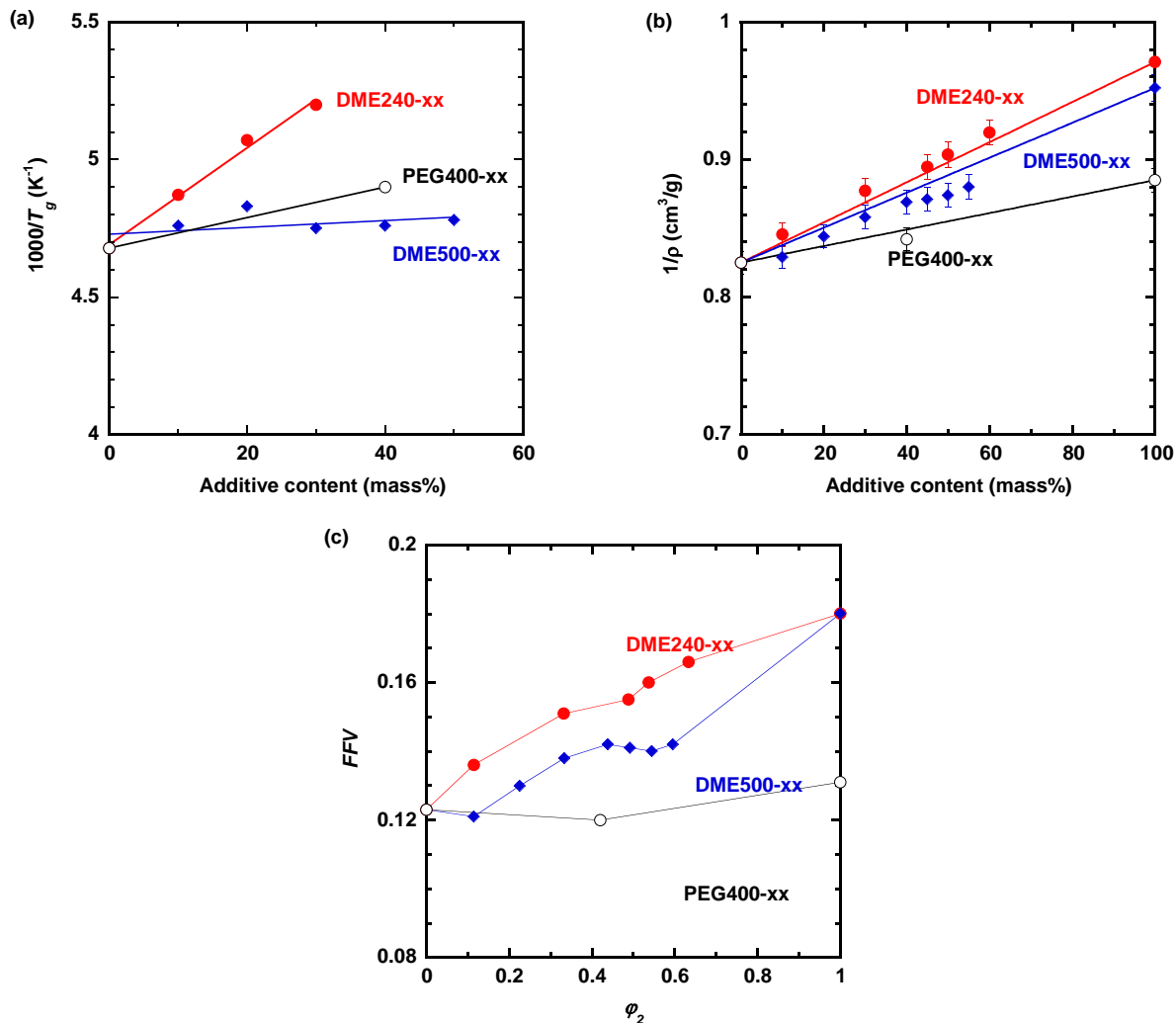
169 Figures 1d and S1 displays the photos of example films of PDXLA and DME240-45. Both
170 films are flexible and mechanically strong for handling. Figure 2c presents the DSC curves of
171 DME240-xx samples. The blends containing PEGDME240 higher than 40 mass% show a melting
172 peak of ≈ 10 $^{\circ}\text{C}$, indicating that the additive induces the polymer crystallization. Nevertheless, all
173 samples are amorphous at 23 $^{\circ}\text{C}$ or above. Figure 3a shows that increasing the PEGDME240
174 content in the blends decreases the T_g because of the plasticization effect. The T_g for the blends
175 containing more than 40% PEGDME240 cannot be observed because the T_g is lower than the
176 testing limit of our equipment (*i.e.*, -90 $^{\circ}\text{C}$). The DSC curves for other blends are displayed in
177 Figure S4a.

178 The T_g of homogeneous blends can be described using Fox Equation [29, 35, 36]:

179
$$1/T_g = w_1/T_{g,1} + w_2/T_{g,2} \quad (5)$$

180 where w is the mass percentage, and the subscripts of 1 and 2 refer to the polymer (PDXLA) and
181 additive, respectively.

182



183 **Figure 3.** Influence of the additive content on (a) the T_g (modeled using Equation 5), (b) density
 184 (modeled using Equation 6), and (c) FFV . The detailed values are summarized in Tables 1 and S1.
 185

186 Figure 3a displays that the T_g of the blends can be satisfactorily described using Equation
 187 5 with the $T_{g,2}$ value of -120 °C for PEGDME240, -67 °C for PEGDME500, and -82 °C for PEG400,
 188 lower than the $T_{g,1}$ of -59 °C. The successful modeling also confirms that the additives are miscible
 189 with PDXLA. PEGDME240 exhibits lower T_g than PEGDME500 and PEG400 because of the
 190 lower molecular weight and the lack of hydrogen bonding. Moreover, the equation predicts the T_g
 191 value of -88 , -92 , and -95 °C for DME240-40, DME240-45, and DME240-50, respectively,
 192 confirming that their T_g 's are too low to detect using our apparatus.

193 **Table 1.** Physical properties of DME240-xx samples, including φ_2 , ρ , T_g , FFV , ether oxygen
 194 content, and CO₂/N₂ separation properties at 3.0 bar.

Samples	φ_2	ρ (g/cm ³)	T_g (°C)	FFV	Oxygen content (mol/L)	Permeability (Barrer)		CO ₂ /N ₂ selectivity
						CO ₂	N ₂	
PDXLA	0	1.212±0.005	-59	0.123	29.1	220	4.0	56
DME240-10	0.12	1.183±0.008	-68	0.136	28.2	380	7.4	51
DME240-30	0.33	1.140±0.005	-81	0.151	26.9	830	17	48
DME240-45	0.49	1.118±0.003	-88*	0.155	26.1	1400	32	45
DME240-50	0.54	1.107±0.008	-92*	0.160	25.8	1700	40	42
PEG400-40	0.42	1.188±0.009	-69	0.120	26.2	360	6.5	56

195 * Estimated using Equation 5.
 196

197 Figure 3b illustrates the impact of the additive loading on the density (ρ). Increasing the
 198 loading decreases the density, and PEGDME240 is most effective in lowering the density among
 199 the three additives, consistent with its lowest T_g . The ρ can be described using the additive model,
 200 as shown below [16]:

$$201 \quad 1/\rho = w_1/\rho_1 + w_2/\rho_2 \quad (6)$$

202 The fitting is satisfactory and does not require any adjustable parameters. The ρ_2 values are
 203 provided by the manufacturers and recorded in Tables 1 and S1. The volume fraction of the
 204 additive (φ_2) can then be estimated using Equation 7:

$$205 \quad \varphi_2 = w_2\rho/\rho_2 \quad (7)$$

206 The φ_2 values are also recorded in Tables 1 and S1.

207 The density can be used to derive fractional free volume (FFV), an important parameter
 208 influencing gas diffusivity, using Equation 8 [37]:

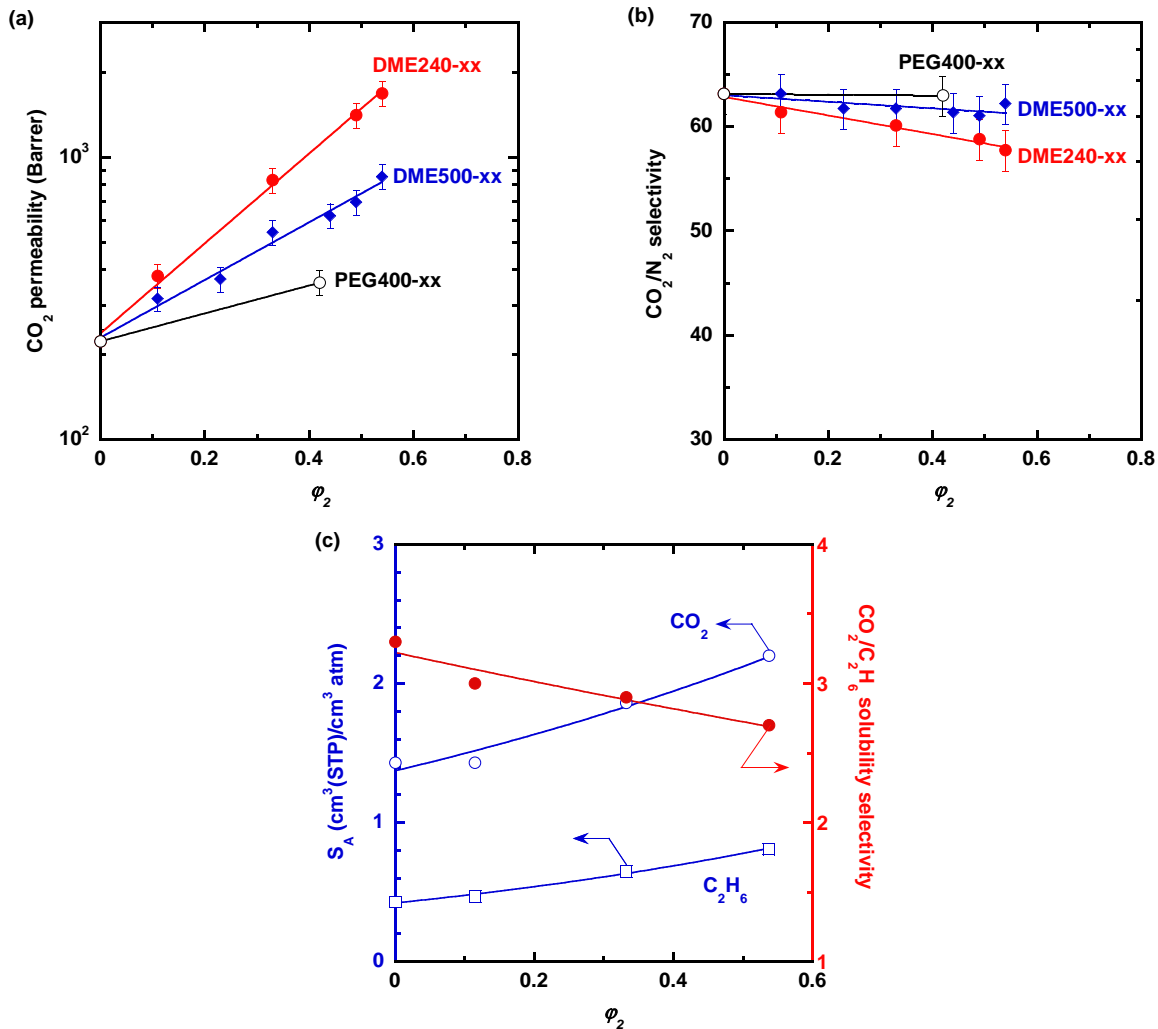
$$209 \quad FFV = \frac{V-V_0}{V} = \frac{V-1.3V_W}{V} \quad (8)$$

210 where V is the specific volume of the polymer, V_0 is the specific occupied volume at 0 K, and V_w
211 is the Van der Waals volume estimated using the group contribution method. The parameters are
212 recorded in Table S2. Figure 3c shows that the FFV increases with the increasing φ_2 because the
213 additives act as a plasticizer. The PEG400-xx have the lowest FFV because the hydrogen bonding
214 between PEG400 and PDXLA (cf. Figure S3) improves the efficiency of the chain packing. The
215 introduction of the PEGDME240 leads to the highest FFV among the three additives, consistent
216 with its lowest T_g and density.

217 **3.2. Pure-gas CO₂/N₂ separation properties**

218 Figure 4a,b exhibits the influence of the φ_2 on pure-gas CO₂ permeability and CO₂/N₂
219 selectivity of the blends at 35 °C, respectively. Increasing the additive concentration increases gas
220 permeability with a slight decrease in CO₂/N₂ selectivity. At the same loading level, gas
221 permeability decreases in the order of DME240-xx, DME500-xx, and PEG400-xx, consistent with
222 the order of decreasing FFV and increasing T_g . The films are also stable after the high-pressure
223 permeation tests. For example, PDXLA has a thickness of $208 \pm 6 \mu\text{m}$ before the test and 207 ± 7
224 μm after the test, while DME240-45 has a thickness of $187 \pm 6 \mu\text{m}$ before the test and $183 \pm 7 \mu\text{m}$
225 after the test despite its high content of PEGDME240.

226



227 **Figure 4.** Impact of the ϕ_2 in the blends on (a) CO₂ permeability, (b) CO₂/N₂ selectivity, and (c)
 228 CO₂ and C₂H₆ solubility coefficient and CO₂/C₂H₆ solubility selectivity at 35 °C (cf. Table S3).
 229 The curves are the best fits of Equation 9.
 230

231 Gas transport properties of homogenous blends can be described by the following
 232 equations [9, 38]:

$$233 \quad \ln \gamma = \phi_1 \ln \gamma_1 + \phi_2 \ln \gamma_2 \quad (9)$$

234 where γ_A can be P_A , S_A , D_A , or their selectivities. As shown in Figure 4a,b, the data for all additives
 235 can be fitted satisfactorily. PEGDME500 is estimated to have CO₂ permeability of 2300 Barrer
 236 and CO₂/N₂ selectivity of 45, consistent with the literature [20, 39]. By contrast, PEGDME240 is

237 estimated to exhibit CO₂ permeability of 9600 Barrer, more than 40 times that of PDXLA, and a
238 moderate CO₂/N₂ selectivity of 35.

239 To elucidate the impact of the additive loading on the gas transport properties, the gas
240 sorption isotherms in DME240-xx at 35°C were determined, as they present the most attractive
241 separation properties. Figure 4c shows the increase of CO₂ solubility with the increasing
242 PEGDME240 loading because of the increased *FFV*, though it is counteracted by the decreased
243 content of the CO₂-philic ether oxygen groups (cf. Figure S4b). For example, DME240-50 exhibits
244 CO₂ solubility of 2.2 cm³(STP) cm⁻³ atm⁻¹, higher than that of PDXLA (1.4 cm³(STP) cm⁻³ atm⁻¹),
245 though DME240-50 shows an ether oxygen content of 25.8 mol/L compared with 29.1 mol/L for
246 PDXLA.

247 C₂H₆ is chosen as a marker for N₂ because N₂ solubility is too low to determine using our
248 apparatus. C₂H₆ does not have specific interactions with the ether oxygen groups (similar to N₂),
249 and thus CO₂/N₂ selectivity is expected to follow a trend similar to CO₂/C₂H₆ solubility selectivity
250 [32]. Figure 4c displays that increasing the loading of PEGDME240 increases the C₂H₆ solubility
251 because of the increased *FFV*, which can also be described using Equation 9 [38]. Nevertheless,
252 the CO₂/C₂H₆ solubility selectivity slightly decreases from 3.3 for PDXLA to 2.7 for DME240-50,
253 which can be ascribed to the decreased content of the CO₂-philic ether oxygen content.

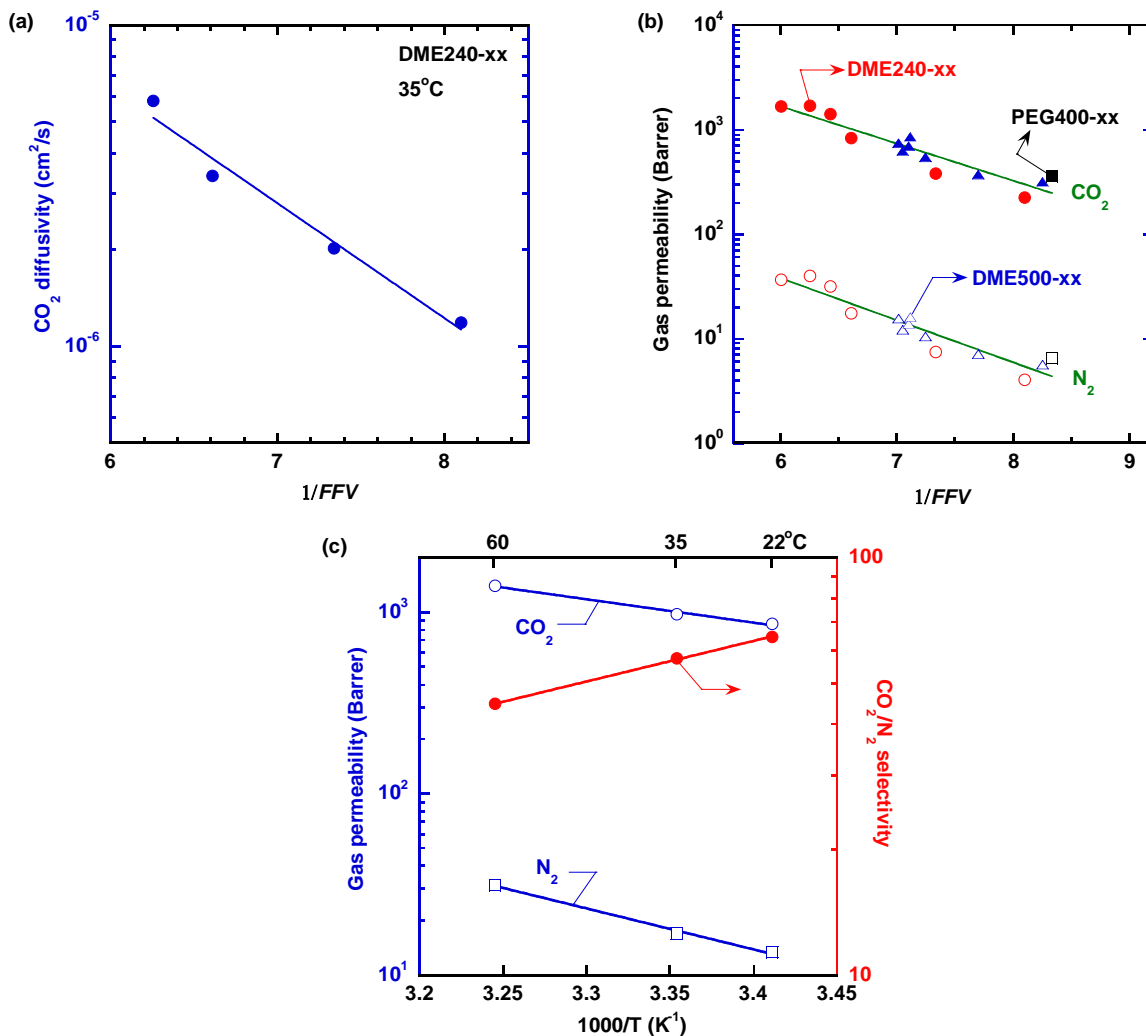
254 3.3. Modeling of gas transport properties using the *T_g*-integrated free volume model

255 CO₂ diffusivity increases with increasing PEGDME240 loading, consistent with the
256 decreased *T_g*. For instance, increasing the PEGDME240 loading from 0 to 50 mass% increases the
257 CO₂ diffusivity from 1.2×10⁻⁶ to 5.8×10⁻⁶ cm²/s (Table S3). Gas diffusivity in polymers can be
258 described using the free volume model [36, 37, 40]:

$$259 \quad D_A = D_{A,0} \exp\left(-\frac{B_A}{FFV}\right) \quad (10)$$

260 where $D_{A,0}$ and B_A are adjustable parameters. Figure 5a demonstrates that the CO₂ diffusivity can
 261 be satisfactorily described using the free volume model.

262



263 **Figure 5.** (a) Correlation between the FFV and CO₂ diffusivity using Equation 10 in DME240-xx
 264 at 35 °C. (b) Correlation between the FFV and N₂ and CO₂ permeability by Equation 11 for
 265 DME240-xx, DME500-xx, and PEG400-xx at 35 °C. (c) Correlation of T and CO₂/N₂ separation
 266 properties in DME240-45 using Equation 12.

267

268 If the FFV has much more influence on D_A than S_A , Equation 10 can be written as:

269

$$P_A = S_A D_{A,0} \exp\left(-\frac{B_A}{FFV}\right) \quad (11)$$

270 This assumption is valid for the DME240-xx. For example, increasing the PEGDME240 loading
271 from 0 to 50 mass% increases the CO₂ solubility by 57% and CO₂ diffusivity by 320%. Figure 5b
272 demonstrates that Equation 11 can be satisfactorily used to describe N₂ and CO₂ permeability in
273 the PDXLA-based blends with three additives, confirming that the change in gas permeability can
274 be ascribed to the change in the free volume.

275 DME240-45 was investigated for gas separation at various temperatures. Figure 5c depicts
276 that increasing the temperature increases gas permeability and decreases gas selectivity, which can
277 be described by the Arrhenius Equation:

$$278 \quad P_A = P_{A,0} \exp\left(\frac{-E_{P,A}}{RT}\right) \quad (12)$$

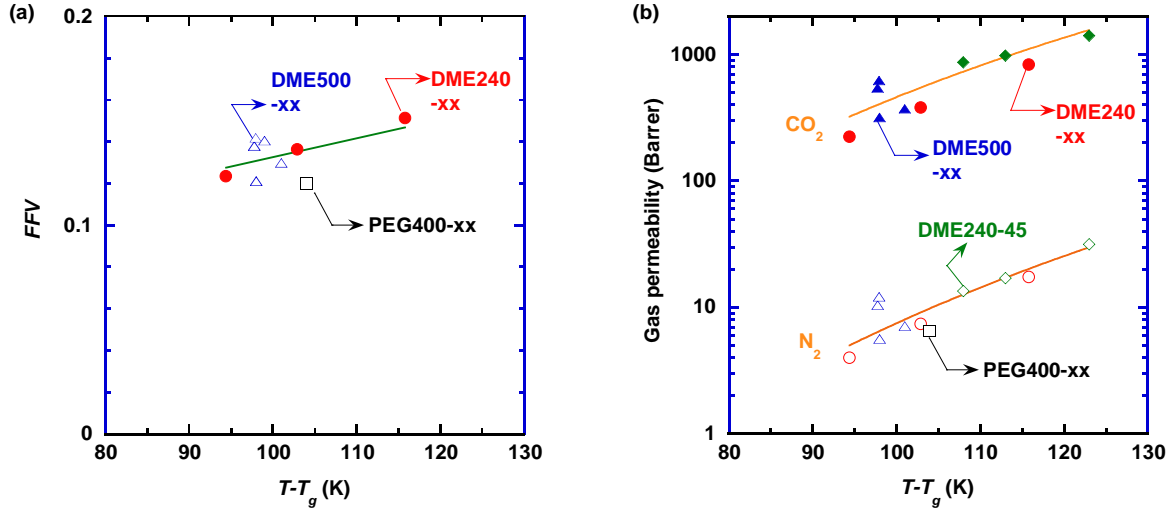
279 where $P_{A,0}$ is the front factor (Barrer), and $E_{P,A}$ is the activation energy of permeation (kJ/mol).
280 The fitting yields the $E_{P,A}$ value of 16 kJ/mol for CO₂ and 30 kJ/mol for N₂, consistent with the
281 greater condensability and smaller kinetic diameter of CO₂ than N₂.

282 For rubbery polymers, FFV can be estimated using Equation 13 [29, 37, 41]:

$$283 \quad FFV = FFV(T_g) + \alpha_r(T - T_g) \quad (13)$$

284 where $FFV(T_g)$ is the apparent FFV at T_g , and α_r is the expansion coefficient of the polymer. Figure
285 6a presents that the FFV of the PDXLA-based samples can be correlated with the T_g with the
286 $FFV(T_g)$ of 0.042 and α_r of $9.0 \times 10^{-4} \text{ K}^{-1}$, which are remarkably consistent with those proposed
287 in the literature (0.025 for $FFV(T_g)$ and $7.8 \times 10^{-4} \text{ K}^{-1}$ for α_r of PEO-based materials) [37].

288



289 **Figure 6.** (a) Correlation between the FFV and T_g for the PDXLA-based polymers using Equation
 290 13. (b) Correlation of N_2 (open symbols) and CO_2 (filled symbols) permeability with T_g using the
 291 T_g -integrated free volume model (Equation 14) for the PDXLA-based blends and DME240-45 at
 292 20, 25, and 35 °C (green symbols).
 293

294 Combining Equations 11 and 13 yields [29, 37, 41]:

$$295 \quad P_A = S_A D_{A,0} \exp\left(\frac{-B_A/\alpha_r}{FFV(T_g)/\alpha_r + (T - T_g)}\right) \quad (14)$$

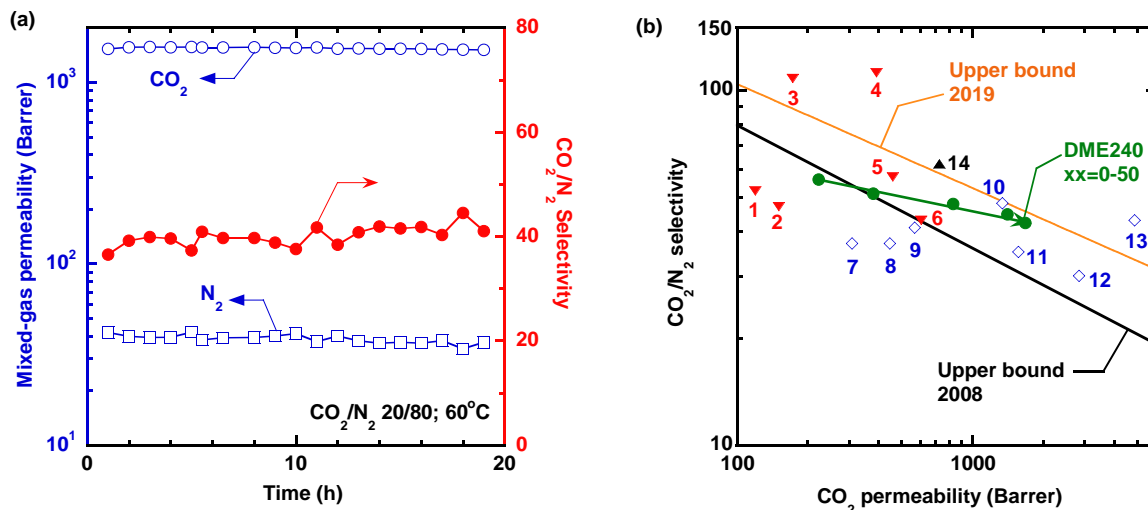
296 This equation is similar to the VTF equation used to describe the ion transport and the
 297 Williams-Landel-Ferry (WLF) equation to model the viscosity of rubbery polymers. The
 298 $FFV(T_g)/\alpha_r$ often has a value of 50 K [42], and the B_A/α_r is related to the activation energy for
 299 diffusion (*i.e.*, $E_{D,A}/R = B_A/\alpha_r$). Equation 14 has been used to interpret gas permeability in PEO-
 300 based copolymers, but not the blends of PDXLA with liquid plasticizers. Figure 6b shows that the
 301 N_2 and CO_2 permeability can be well correlated with $(T - T_g)$, which is impressive considering that
 302 the data include permeability for DME240-xx, DME500-xx, and PEG400-xx at 35 °C and
 303 DME240-45 at 20, 25, and 35 °C.

304 3.4. Superior CO_2/N_2 separation performance in DME240-45

305 The DME240-45 was further evaluated with model flue gas containing CO_2/N_2 of 20/80 at
 306 7.9 bar and 60 °C. Figure 7a displays that the DME240-45 exhibits mixed-gas CO_2 permeability

307 of 1540 Barrer, N₂ permeability of 39 Barrer, and CO₂/N₂ selectivity of 40. The CO₂/N₂ separation
 308 performance is stable during the 20-h test at 60 °C. Nevertheless, a longer-term demonstration of
 309 the stability of these blends will be needed for them to be considered for practical applications.

310



311 **Figure 7.** Superior CO₂/N₂ separation properties of DME240. (a) Mixed-gas separation
 312 performance of DME240-45 with CO₂/N₂ of 20/80 at 7.9 bar and 60 °C. (b) Comparison of
 313 DME240-xx (●) in Robeson's 2008 and 2019 upper bounds with other leading polyethers [43],
 314 including Pebax-based blends (▼) [13, 14, 19-21, 44], cross-linked PEO-based blends (◇) [9, 17,
 315 23, 24, 27, 29, 39], and PDXLA-co-PDXLEA (▲) [32]. The details for these polyethers are
 316 summarized in Table S4.

317

318 Figure 7b compares the CO₂/N₂ separation properties of the DME240-xx with Robeson's
 319 2008 and 2019 upper bounds at 35 °C (*i.e.*, the tradeoff between permeability and selectivity) [43].
 320 The DME240-45 and DME240-50 exhibit CO₂/N₂ separation properties above the 2008 upper
 321 bound and close to the 2019 one. Specifically, the DME240-50 shows CO₂ permeability of 1680
 322 Barrer and CO₂/N₂ selectivity of 42, comparable with the leading polyethers in the literature,
 323 including those loaded with PEGDME [17, 24, 27, 39, 44].

324

325 4. Conclusion

326 We demonstrate by experimentation and modeling that PDXLA can be blended with
327 miscible additives (including PEG400, PEGDME240, and PEGDME500) to enhance CO₂
328 permeability while retaining the high CO₂/N₂ selectivity. Increasing the additive content decreases
329 the density and T_g , which can be satisfactorily described using the additive model and Fox equation,
330 respectively. More importantly, the effect of the additive content and testing temperature on gas
331 permeability and selectivity can be described using a T_g -integrated free volume model. Among the
332 three additives, PEGDME240 renders the most significant impact on the T_g , FFV , and gas
333 permeability because of its lowest T_g and highest FFV and the absence of hydrogen bonding.
334 DME240-45 exhibiting excellent CO₂/N₂ separation properties was further evaluated with model
335 flue gas and demonstrates the separation performance above Robeson's 2008 upper bound,
336 indicating its potential for practical applications. This work lays out a theoretical foundation for a
337 facile and fruitful way to improve gas separation properties by designing thermally stable
338 homogeneous blends.

339

340 **ACKNOWLEDGMENT**

341 This work was financially supported by the U.S. Department of Energy (DE-
342 FE0031736), the New York State Foundation for Science, Technology, and Innovation
343 (NYSTAR), and the U.S. National Science Foundation (1554236).

344

345 **REFERENCES**

- 346 [1] Y. Han, W. S. Ho. Polymeric membranes for CO₂ separation and capture. *J. Membr. Sci.*
347 628 (2021) 119244.
348 [2] L. Hu, K. Clark, T. Alebrahim, H. Lin. Mixed matrix membranes for post-combustion
349 carbon capture: From materials design to membrane engineering. *J. Membr. Sci.* 644 (2022)
350 120140.

- 351 [3] M. Galizia, W. S. Chi, Z. P. Smith, T. C. Merkel, R. W. Baker, B. D. Freeman. 50th
352 Anniversary perspective: Polymers and mixed matrix membranes for gas and vapor
353 separation: A review and prospective opportunities. *Macromolecules*. 50 (2017) 7809-
354 7843.
- 355 [4] S. Roussanaly, R. Anantharaman, K. Lindqvist, H. Zhai, E. Rubin. Membrane properties
356 required for post-combustion CO₂ capture at coal-fired power plants. *J. Membr. Sci.* 511
357 (2016) 250-264.
- 358 [5] B. Zhu, X. Jiang, S. He, X. Yang, J. Long, Y. Zhang, L. Shao. Rational design of
359 poly(ethylene oxide) based membranes for sustainable CO₂ capture. *J. Mater. Chem. A*. 8
360 (2020) 24233-24252.
- 361 [6] J. Liu, X. Hou, H. Park, H. Lin. High-performance polymers for membrane CO₂/N₂
362 separation. *Chem. Eur. J.* 22 (2016) 15980-15990.
- 363 [7] C. G. Rodriguez, M. Chwatko, J. Park, C. L. Bentley, B. D. Freeman, N. A. Lynd.
364 Compositionally controlled polyether membranes via mono(mu-
365 alkoxo)bis(alkylaluminum)-Initiated chain-growth network epoxide polymerization:
366 synthesis and transport properties. *Macromolecules*. 53 (2020) 1191-1198.
- 367 [8] V. A. Kusuma, B. D. Freeman, M. A. Borns, D. S. Kalika. Influence of chemical structure
368 of short chain pendant groups on gas transport properties of cross-linked poly(ethylene
369 oxide) copolymers. *J. Membr. Sci.* 327 (2009) 195-207.
- 370 [9] H. Lin, E. V. Wagner, J. S. Swinnea, B. D. Freeman, S. J. Pas, A. J. Hill, S. Kalakkunnath,
371 D. S. Kalika. Transport and structural characteristics of crosslinked poly(ethylene oxide)
372 rubbers. *J. Membr. Sci.* 276 (2006) 145-161.
- 373 [10] Y. Hirayama, Y. Kase, N. Tanihara, Y. Sumiyama, Y. Kusuki, K. Haraya. Permeation
374 properties to CO₂ and N₂ of poly(ethylene oxide)-containing and crosslinked polymer films.
375 *J. Membr. Sci.* 160 (1999) 87-99.
- 376 [11] W. Yave, H. Huth, A. Car, C. Schick. Peculiarity of a CO₂-philic block copolymer confined
377 in thin films with constrained thickness: "A super membrane for CO₂-capture". *Energy*
378 *Environ. Sci.* 4 (2011) 4656-4661.
- 379 [12] S. R. Reijerkerk, M. H. Knoef, K. Nijmeijer, M. Wessling. Poly(ethylene glycol) and
380 poly(dimethyl siloxane): Combining their advantages into efficient CO₂ gas separation
381 membranes. *J. Membr. Sci.* 352 (2010) 126-135.
- 382 [13] V. I. Bondar, B. D. Freeman, I. Pinnau. Gas transport properties of poly(ether-*b*-amide)
383 segmented block copolymers. *J. Polym. Sci.: Part B: Polym. Phys.* 38 (2000) 2051-2062.
- 384 [14] B. Zhang, C. Yang, Y. Zheng, Y. Wu, C. Song, Q. Liu, Z. Wang. Modification of CO₂-
385 selective mixed matrix membranes by a binary composition of poly(ethylene glycol)/NaY
386 zeolite. *J. Membr. Sci.* 627 (2021) 119239.
- 387 [15] J. Liu, C. R. P. Fulong, L. Hu, L. Huang, G. Zhang, T. R. Cook, H. Lin. Interpenetrating
388 networks of mixed matrix materials comprising metal-organic polyhedra for membrane
389 CO₂ capture. *J. Membr. Sci.* 606 (2020) 118122.
- 390 [16] L. Hu, J. Liu, L. Zhu, X. Hou, L. Huang, H. Lin, J. Cheng. Highly permeable mixed matrix
391 materials comprising ZIF-8 nanoparticles in rubbery amorphous poly(ethylene oxide) for
392 CO₂ capture. *Sep. Purif. Techn.* 205 (2018) 58-65.
- 393 [17] X. Jiang, S. Li, L. Shao. Pushing CO₂-philic membrane performance to the limit by
394 designing semi-interpenetrating networks (SIPN) for sustainable CO₂ separations. *Energy*
395 *Environ. Sci.* 10 (2017) 1339-1344.

- 396 [18] J. Shen, G. Liu, K. Huang, W. Jin, K. R. Lee, N. Xu. Membranes with fast and selective
397 gas-transport channels of lamellar graphene oxide for efficient CO₂ capture. *Angew. Chem.*
398 *Int. Ed.* 127 (2015) 588-592.
- 399 [19] R. He, S. Cong, S. Xu, S. Han, H. Guo, Z. Liang, J. Wang, Y. Zhang. CO₂-philic mixed
400 matrix membranes based on low-molecular-weight polyethylene glycol and porous organic
401 polymers. *J. Membr. Sci.* 624 (2021) 119081.
- 402 [20] W. Yave, A. Car, K.-V. Peinemann. Nanostructured membrane material designed for
403 carbon dioxide separation. *J. Membr. Sci.* 350 (2010) 124-129.
- 404 [21] A. Car, C. Stropnik, W. Yave, K.-V. Peinemann. PEG modified poly(amide-b-ethylene
405 oxide) membranes for CO₂ separation. *J. Membr. Sci.* 307 (2008) 88-95.
- 406 [22] N. P. Patel, R. J. Spontak. Mesoblends of polyether block copolymers with poly(ethylene
407 glycol). *Macromolecules.* 37 (2004) 1394-1402.
- 408 [23] W. Sun, M. Yin, W. Zhang, S. Li, N. Wang, Q. An. Green techniques for rapid fabrication
409 of unprecedentedly high-performance PEO membranes for CO₂ capture. *ACS Sustain.*
410 *Chem. Eng.* 9 (2021) 10167-10175.
- 411 [24] S. Li, X. Jiang, X. Yang, Y. Bai, L. Shao. Nanoporous framework “reservoir” maximizing
412 low-molecular-weight enhancer impregnation into CO₂-philic membranes for highly-
413 efficient CO₂ capture. *J. Membr. Sci.* 570-571 (2019) 278-285.
- 414 [25] J. Cheng, L. Hu, Y. Li, C. Ji, J. Zhou, K. Cen. Improving CO₂ permeability of ceramic
415 hollow fibre-supported composite membranes by blending an ionic liquid in the
416 Pebax/PEGDME selective layer. *RSC Adv.* 6 (2016) 2055-2064.
- 417 [26] H. Chen, T. S. Chung. CO₂-selective membranes for hydrogen purification and the effect
418 of carbon monoxide (CO) on its gas separation performance. *J. Membr. Sci.* 37 (2012)
419 6001-6011.
- 420 [27] S. Quan, S. Li, Z. Wang, X. Yan, Z. Guo, L. Shao. A bio-inspired CO₂-philic network
421 membrane for enhanced sustainable gas separation. *J. Mater. Chem. A.* 3 (2015) 13758-
422 13766.
- 423 [28] W. Yave, A. Car, S. S. Funari, S. P. Nunes, K. V. Peinemann. CO₂-philic polymer
424 membrane with extremely high separation performance. *Macromolecules.* 43 (2010) 326-
425 333.
- 426 [29] L. Huang, J. Liu, H. Lin. Thermally stable, homogeneous blends of cross-linked
427 poly(ethylene oxide) and crown ethers with enhanced CO₂ permeability. *J. Membr. Sci.*
428 610 (2020) 118253.
- 429 [30] T. Alebrahim, A. Chakraborty, L. Hu, S. Patil, S. Cheng, D. Acharya, C. M. Doherty, A. J.
430 Hill, T. R. Cook, H. Lin. Gas transport characteristics of supramolecular networks of metal-
431 coordinated highly branched poly(ethylene oxide). *J. Membr. Sci.* 644 (2022) 120063.
- 432 [31] S. Meshkat, S. Kaliaguine, D. Rodrigue. Enhancing CO₂ separation performance of
433 Pebax® MH-1657 with aromatic carboxylic acids. *Sep. Purif. Techn.* 212 (2019) 901-912.
- 434 [32] J. Liu, S. Zhang, D. Jiang, C. M. Doherty, A. J. Hill, C. Cheng, H. Park, H. Lin. Highly
435 polar but amorphous polymers with robust membrane CO₂/N₂ separation performance.
436 *Joule.* 3 (2019) 1881-1894.
- 437 [33] L. Huang, W. Guo, H. Mondal, S. Schaefer, T. N. Tran, H. Lin. Effect of the branch length
438 on structural and CO₂/N₂ separation properties of hyperbranched poly(1,3-dioxolane).
439 *Macromolecules.* 55 (2022) 382-389.

- 440 [34] J. Liu, G. Zhang, K. Clark, H. Lin. Maximizing ether oxygen content in polymers for
441 membrane CO₂ removal from natural gas. *ACS Appl. Mater. Interfaces*. 11 (2019) 10933-
442 10940.
- 443 [35] W. Brostow, R. Chiu, I. M. Kalogeras, A. Vassilikou-Dova. Prediction of glass transition
444 temperatures: Binary blends and copolymers. *Mater. Lett.* 62 (2008) 3152-3155.
- 445 [36] H. Lin, M. Yavari. Upper bound of polymeric membranes for mixed-gas CO₂/CH₄
446 separations. *J. Membr. Sci.* 475 (2015) 101-109.
- 447 [37] H. Lin, B. D. Freeman, S. Kalakkunnath, D. S. Kalika. Effect of copolymer composition,
448 temperature, and carbon dioxide fugacity on pure- and mixed-gas permeability in
449 poly(ethylene glycol)-based materials: Free volume interpretation. *J. Membr. Sci.* 291
450 (2007) 131-139.
- 451 [38] D. R. Paul. Gas transport in homogeneous multicomponent polymers. *J. Membr. Sci.* 18
452 (1984) 75-86.
- 453 [39] Z. Dai, H. Aboukeila, L. Ansaloni, J. Deng, M. Giacinti Baschetti, L. Deng. Nafion/PEG
454 hybrid membrane for CO₂ separation: Effect of PEG on membrane micro-structure and
455 performance. *Sep. Purif. Techn.* 214 (2019) 67-77.
- 456 [40] J. Park, D. R. Paul. Correlation and prediction of gas permeability in glassy polymer
457 membrane materials via a modified free volume based group contribution method. *J.*
458 *Membr. Sci.* 125 (1997) 23-39.
- 459 [41] V. A. Kusuma, J. S. McNally, J. S. Baker, Z. Tong, L. Zhu, C. J. Orme, F. F. Stewart, D.
460 P. Hopkinson. Cross-linked polyphosphazene blends as Robust CO₂ separation membranes.
461 *ACS Appl. Mater. Interfaces*. 12 (2020) 30787-30795.
- 462 [42] Y. Karatas, R. D. Banhatti, N. Kaskhedikar, M. Burjanadze, K. Funke, H.-D. Wiemhöfer.
463 Synthesis and modeling of polysiloxane-based salt-in-polymer electrolytes with various
464 additives. *J. Phys. Chem. B*. 113 (2009) 15473-15484.
- 465 [43] B. Comesaña-Gándara, J. Chen, C. G. Bezzu, M. Carta, I. Rose, M.-C. Ferrari, E. Esposito,
466 A. Fuoco, J. C. Jansen, N. B. McKeown. Redefining the Robeson upper bounds for
467 CO₂/CH₄ and CO₂/N₂ separations using a series of ultrapermeable benzotriptycene-based
468 polymers of intrinsic microporosity. *Energy Environ. Sci.* 12 (2019) 2733-2740.
- 469 [44] N. Liu, J. Cheng, L. Hu, W. Hou, X. Yang, M. Luo, H. Zhang, B. Ye, J. Zhou. Boosting
470 CO₂ transport of poly(ethylene oxide) membranes by hollow Rubik-like “expressway”
471 channels with anion pillared hybrid ultramicroporous materials. *Chem. Eng. J.* 427 (2022)
472 130845.

473